RSC Applied Interfaces

Accepted Manuscript

This article can be cited before page numbers have been issued, to do this please use: A. R. N. Aouichaoui, D. Tisi, I. E. Castelli and A. Bhowmik, *RSC Appl. Interfaces*, 2026, DOI: 10.1039/D6LF00149A.

ROYAL SOCIETY OF CHEMISTRY

rsc.li/RSCApplInter

View Article Online
DOI: 10.1039/D6LF00149A

Journal Name

ARTICLE TYPE

Cite this: DOI: 00.0000/xxxxxxxxxx

Machine Learning Potentials for Electrified Interfaces†

Adem R. N. Aouichaoui*, Davide Tisi, Ivano E. Castelli*, and Arghya Bhowmik*[a]

Received Date
Accepted Date

DOI: 00.0000/xxxxxxxxxx

Accurate atomistic modelling of electrochemical interfaces requires accounting for applied electrode potential and performing molecular dynamics at constant potential. The computational cost of grand-canonical density functional theory restricts simulations to small system sizes and short timescales. Machine learning interatomic potentials (MLIPs) have been proven useful for long time and large length scale simulations, but their generalisation to and applicability at electrified interfaces have yet to be widely demonstrated and adopted. In this perspective, we review emerging approaches for developing MLIPs for systems under applied potential, organising them into two categories: (i) linear response methods that learn response properties (electronegativities, Born charges, polarisabilities) and compute energies through physics-based expansions, and (ii) direct learning methods that take the applied electrochemical potential as input variable and learn the potential-dependent energy surface end-to-end. We identify key challenges including training data scarcity, lack of standardisation, and architectural limitations in current MLIPs. To address these issues, we propose flexible templates for incorporating global electrochemical information into MLIP architectures, and data-efficient strategies such as transfer learning and multi-head architectures that leverage abundant existing zero-potential data. We conclude by calling for community initiatives to establish shared datasets and reporting standards for electrified interfaces.

1 Introduction

Critical energy conversion and storage processes rely on electrochemical transformation at the solid-liquid interface [1]. The ability to understand and model interfacial phenomena in electrocatalysis is key in the design and optimisation of current and future green technologies [2,3]. In fact, electrocatalysis plays a central role in a wide range of applications such as oxygen reduction reactions(ORR)in fuel cells [4], hydrogen evolution reactions (HER) occurring during water splitting in electrolysis [5,6], CO_2 and N_2reduction reactions (CO_2RR/N_2RR) [7,8] in electrochemical converters as well as electrochemical reactions in batteries [9,10].

The presence of external electric fields can drastically modify atomic and electronic structure of the interfaces and provide the crucial driving force for many of the electrochemical processes, including catalytic reactions. Electric fields can directly modulate the distribution of charge, the orientation of polar species, the stabilisation of transition states, and the energetics of surface bound reaction intermediates. At the catalytic interface i.e. the electrochemical double layer, the local electric field can shift adsorption equilibria and alter reaction pathways [11–14].

Applied potential significantly alters the structure and dynamics of ions and polarisable solvents at the interface, affecting their reorganisation and modifying the pathways and barriers for electron and proton transfer [15]. Accurate representation of atomic and electronic processes at the Helmholtz layer requires that atomistic simulations explicitly consider these effects of applied potential [16,17]. Density functional theory (DFT) based simulations offer accurate microscopic insights, but the computational cost limits the system sizes and timescales that can be studied [18]. In recent decades, machine-learning interatomic potentials (MLIPs) have emerged as a promising solution to this cost-accuracy trade-off: once trained on high-quality quantum-mechanical reference data, MLIPs can approach DFT accuracy at a computational cost only marginally higher than that of classical force fields [19–31]. This has enabled longer simulation times and the ability to examine larger systems, which is important modelling and sampling of interactions driving complex catalytic reactions [32]. However, despite the substantial progress in MLIP architectures, the optimal strategy for incorporating explicit electric-field contributions remains unclear [33] but remains as a critical requirement of MLIPs to be used to demystify the mechanisms observed in electrochemical interfaces [34,35].

In this perspective we will layout the current status in simulating interfaces under applied potential, highlighting the challenges from three different perspectives: i) first-principle computational methods along with the cost associated with data generation, ii) the lack of large standardised repositories for such data and iii) the lack of readily available applied potential aware ma-

[a] Department of Energy Conversion and Storage, Technical University of Denmark, Agnes Nielsens Vej 301, 2800 Kgs. Lyngby, Denmark; E-mail: arnaou@dtu.dk, ivca@dtu.dk, arbh@dtu.dk

View Article Online
DOI: 10.1039/D6LF00149A

chine learning (ML) models for such applications.

2 First-principle Methods for Electrified SLI

DFT simulations represent the state of the art technique in studying complex interactions pertaining to electrochemical interfaces. However, to achieve realistic cost of *ab-initio* simulations for electrochemically relevant systems, current approaches rely on a range of assumptions and approximations, whose impact on the physical validity of the simulation outcome is often unclear and system dependent. An in-depth analysis of these methods and their limitations has been the focus of many other studies[32,36]. The details being beyond the scope of this article, here we give an overview of the challenges. Electrified SLI can be studied by both constant potential or constant charge methods, which both suffer from the balancing of cost and accuracy. The computational hydrogen electrode (CHE) method[37], is the most simplified one based on vacuum calculations, and is computationally affordable, however it cannot deal with partial charge transfer. Implicit solvation methods approximate the solvent as a continuum dielectric medium that can screen the Coulomb potential between charged particles. Fully *ab-initio* methods for SLI treat both solid surface and the electrolyte explicitly, thus including all the relevant microscopic effects and interactions but increasing the computational cost of the simulation. For this reason, *ab-initio* explicit-solvent DFT methods have an explicit treatment of only the atoms of the electrolyte at the interface and use an implicit solvation cavity as a countercharge to make the overall simulation cell charge neutral. Even with this trade-off, simulations are limited to hundreds of atoms for few tens of picoseconds (ps). As such, there is an urgent need to accelerate such simulations. There is a rich precedence of accelerating *ab-initio* molecular dynamics (AIMD) using machine learning surrogate model for non-electrified systems[38–40], MLIP-accelerated SLI studies that include the effects of applied potentials are still missing.

3 Emerging MLIP for Electrified SLI

In this section, we review recent efforts towards using ML for the modelling of SLIs under applied potential. We organise these developments according to their underlying physical principle for incorporating electric field or applied potential effects. Broadly, current approaches can be categorised into two classes: (i) linear response approaches and learning of the response functions, and (ii) direct learning of the potential-dependent energy surface.

3.1 Linear response approaches

This class of models leverages linear response theory to compute the response of materials to external fields, targeting response functions such as polarisation, polarisability, or Born effective charges. In the loss function, they explicitly include one of these response functions for training. The response function can be predicted with a separate model or part of the same architecture predicting the unperturbed energy. In linear response, the dynamics ara determined by the forces in the perturbed system, $\mathbf{F}_E$, which are obtained as a sum of two terms:

$$\mathbf{F}_E = \mathbf{F}_0 + Z^* E \tag{1}$$

where $\mathbf{F}_0$ is the force contribution without field and $Z^* = \frac{\partial P}{\partial r}$ is the Born effective charges[41] (BEC) and P is the polarization.

Joll *et al.*[42] developed the Perturbed Neural Network Potential (PNNP) to model the effects of external electric fields on condensed phase systems, demonstrating its capabilities on bulk water. The total force on each atom is obtained from Eq. 1. The main characteristic of this approach is the use of two distinct models: a committee of 2^{nd} generation high-dimensional Neural Network potentials (c-NNP) for the unperturbed potential, and an E(3)-equivariant graph neural network to model BEC, called Atomic Polar Tensor (APT). Importantly, both models are trained without the presence of an external electric field. The field is not used as an input to the model, but rather the field-induced forces are computed analytically from the learned APT. The model has shown strong predictive capabilities for electric field strengths ranging from approximately 0.002 to 0.2 V Å^{-1}, with a reported root mean squared error (RMSE) on forces of about 90 meV Å^{-1} at 0.2 V Å^{-1} applied field strength. However, the contribution from the field-induced force to the RMSE increases in proportion with the field strength, reflecting the limitations of the first-order truncation. Additionally, the model only accounts for homogeneous external electric fields throughout the bulk liquid, which may not capture the spatially varying fields present at real electrochemical interfaces.

Falletta *et al.*[43] proposed a unified and differentiable framework for learning materials response to electric fields based on the Allegro[44] local equivariant architecture. Using the atomic positions and the external electric field as input, they leverage automatic differentiation to compute the response properties as exact derivatives of a generalised potential energy. In addition to predicting DFT energies and forces, the loss function explicitly targets the Born effective charges and polarisability, computed using density functional perturbation theory. These quantities are then computed analytic derivatives by the model following the linear response theory. The approach simultaneously learns the electric enthalpy, forces, polarisation, Born charges, and polarisability from the atomic numbers, positions, and electric field. The method has been validated by computing the vibrational and dielectric properties of αSiO_2, and ferroelectric properties of $BaTiO_3$.

Zhang and Jiang[45] proposed the Field-Induced Recursively Embedded Atom Neural Network (FIREANN), which introduces a field-dependent feature directly into the atomic environment descriptor. The approach constructs a field-induced embedded atom density (FI-EAD) by combining Gaussian-type orbitals (GTOs) that depend on neighboring atoms with a field-dependent orbital $\varphi_{l_x,l_y,l_z}(\vec{\varepsilon}) = (\varepsilon_x)^{l_x}(\varepsilon_y)^{l_y}(\varepsilon_z)^{l_z}$, where $\vec{\varepsilon} = (\varepsilon_x, \varepsilon_y, \varepsilon_z)$ is the applied electric field vector. These components are linearly combined into a joint orbital whose squared magnitude forms the FI-EAD feature, capturing system-field interactions while maintaining rotational equivariance. The model intrinsically describes response properties up to arbitrary order by taking analytical gradients of the potential energy with respect to the field vector: the dipole moment $\mu = -\partial E/\partial \varepsilon$ and polarisability $\alpha = -\partial^2 E/\partial \varepsilon \partial \varepsilon$. These properties can be simultaneously learned by including them in the loss function. For liquid water, the authors demonstrated that

View Article Online
DOI: 10.1039/D6LF00149A

training on atomic forces only can bypass the multi-valued polarisation issue in periodic systems while still yielding accurate dipole moments and IR spectra. The model achieved force RMSEs of 39.4 meV Å^{-1} for bulk water under fields up to 0.6 V Å^{-1}.

Feng and Jiang [46] extended the FIREANN [45] framework to accelerate finite-field simulations of electrochemical interfaces. It combines two ML models trained entirely on first-principles data without employing classical approximations for either the electrode or electrolyte. The first model employs the FI-EAD descriptor to predict atomic forces under applied electric fields, with a message-passing-like iteration scheme that updates combination coefficients based on local environments, incorporating higher-order and non-local interactions essential for electrostatic effects at interfaces. Under periodic boundary conditions with an applied field the polarisation is multivalued, rendering absolute energies ill-defined. Thus only atomic forces serve as training targets. The second model, termed MLEDR [47] (Machine Learning Electron Density Response), predicts the field-induced charge redistribution $\Delta n(r;\vec{\varepsilon}) = n_{metal-electrolyte} - n_{metal}(r) - n_{electrolyte}(r)$ at general grid point r_i, not only at the atoms characterised by FI-EAD features but over surrounding real atoms, enabling direct calculation of the Helmholtz capacitance. Validated on the Au(100)/Water interface (with 5.5 M concentration NaCl, 400 atoms) with reference data from finite-field DFT (CP2K package, PBE-D3 functional) across cell potentials of 0-2 V, the approach [46] achieved force RMSEs of approximately 43 meV/Å using 12,139 configurations assembled via active learning, and demonstrated a speedup of roughly four orders of magnitude compared to ab initio molecular dynamics. The model extrapolated reliably to cell potentials of $\pm$4 V, accurately predicting a Helmholtz capacitance of approximately 20.8 μF/cm^2 at the potential of zero charge and revealing a turnover in interfacial water orientation at the anode above 2.5 V arising from competition between the positively charged electrode and specifically adsorbed Cl^- ions.

Bergmann *et al.* [48] developed the Response Analysis in z-ORientation (RAZOR) approach, which extends standard MLIPs to electrified interfaces by machine-learning first-order response parameters. Rather than treating the applied potential as a post-processing correction, RAZOR explicitly learns the work function $\phi_0 = \partial E/\partial q$ and Born effective charges $Z_i^* = \partial F_i/\partial q$ at zero charge, enabling a second-order Taylor expansion of energies and forces as functions of excess charge q. Training requires DFT calculations at $q = 0$, $+q$, and $-q$ for each structure. This approach in theory would triple the require DFT calcualtions, but as pointed out by the authors the use of the charge-neutral electron density to initialize the SCF cycle for the charged calculations reduces this overhead to less than a factor of two in practice. The second-order electronic capacitance is approximated using an implicit solvation model to capture the double layer response. This approach yields charge-dependent atomic forces during molecular dynamics (MD) simulations, allowing proper structural relaxation at applied bias. Applied to describing the dynamics of Cu(100) surface with adsorbed OH, the model achieved an RMSE of 2 meV/atom on the energy prediction and an RMSE of 16 meV on the forces.

3.2 Direct Learning of the Potential-Dependent Energy Surface

The second class of methods takes an end-to-end approach: the applied potential, electric field, or electron number is provided as a direct input to the model, which learns the full configuration - and potential - dependent energy surface without explicit decomposition into response terms. This approach makes no assumptions about the functional form of the potential dependence, allowing the neural network to capture arbitrarily complex (including non-linear) effects.

Zhou *et al.* [33] developed an explicit electric potential machine learning force-field (EEP-MLFF) model for MD simulation, demonstrating its application to Cu cluster formation on MoS_2. The atomic environment is described using the Smooth SO(3) power spectrum descriptor, and the electric potential (U vs. SHE) is concatenated directly to this representation before being fed into a multilayer perceptron. The model treats the potential as simply another input feature, allowing it to learn how the energy surface changes across different electrochemical conditions. The model achieved a satisfactory accuracy with MAE of 4.4 meV/atom for energies and 58.3 meV/Å for forces on their test set, training over 3,897 data point, which however were distributed over a quite narrow potential range of -0.5-0.6 V (vs. SHE), without resting to strong values of the potential.

Wang *et al.* [49] developed a constant potential machine learning force field (CP-MLFF) based on MACE [50] for simulating interfaces in the grand canonical ensemble, where the system exchanges electrons with an external reservoir. The model uses the total electron number N_e as the state variable to predict energies, forces, and the Fermi level. Two architectural strategies are proposed for incorporating N_e:

1. **Node augmentation:** N_e is concatenated with the one-hot encoded element type for each atom before passing through the embedding layer, producing N_e-dependent initial node features that propagate through the message-passing layers.

2. **Global feature:** N_e is embedded into a separate high-dimensional latent space as a graph-level attribute. At each message-passing layer, this global feature is projected and injected into the node features, while simultaneously being updated by aggregating node information through mean pooling. This creates bidirectional information flow between local atomic environments and the global electrochemical state.

The study applied CP-MLFF to CO_2 reduction on a Ni-N-C catalyst at 0.827 V vs. RHE, demonstrating the viability of the approach for constant-potential simulations.

Sun *et al.* [51] are the first to investigate the effects of nuclear quantum effects (NQEs) at electrode interface, via a grand canonical path integral hybrid Monte Carlo (GC-PIHMC) framework. The study employ a modified Deep Potential model [21,52] called DP-N_e that introduces the total number of electrons N_e as an additional input, concatenated to the embedded representation. The model also predicts, with no further computational cost, the work function as an additional output: $\partial E(R,N_e) = -W(R,N_e)$. This allows the model to learn how the electronic chemical potential

View Article Online
DOI: 10.1039/D6LF00149A

responds to changes in configuration and charge state. The total RMSE on the testing dataset are 0.6 meV/atom and 57 meV/Å for the Volmer reaction path, and 1.1 meV/atom and 71 meV/Å for the Heyrovsky reaction. Using this framework, the authors demonstrated that proton tunneling reduces the activation energy by 0.09-0.13 eV at room temperature for HER on Pt(111), and that neglecting NQEs leads to underestimation of reaction rates by 50-100 fold at 300 K.

Chen *et al.* [53] developed a dual-learning scheme for ML emulation of electronically grand-canonical calculations. The approach employs two coupled neural networks based on Behler-Parrinello symmetry functions[23,54]: one predicts per-atom charges $\hat{q}_i$ from atomic positions and electrode potential, while the other predicts per-atom electronegativities $\hat{\chi}_i$ from geometry alone. To incorporate the electrode potential into the descriptor, the authors extend standard symmetry functions with potential-dependent terms of the form $G^{\phi}_{i,k} = \phi \cdot e^{-\eta_k(z_i - z_{\text{surface}})}$, where ϕ is the electrode potential (taken as the work function), z_i is the vertical position of i-th atom normal to the electrode surface, z_{surface} defines the electrode-electrolyte interface, and η_k are decay constants that control the spatial extent of the field influence. The exponential decay with distance from the electrode surface mimics the spatial profile of the electric field as described by Gouy-Chapman model[53]. The grand-canonical energy (Ω) is computed through a physics-based charge-electronegativity expansion:

$$\hat{\Omega} = \sum_{i=1}^{N} \left(E^{0,Z(i)} + (\hat{\chi}_i + \mu_e)\hat{q}_i + \frac{1}{2} J^{Z(i)} \hat{q}_i^2 \right) \tag{2}$$

where $\hat{\chi}_i$ represents the environment-dependent atomic electronegativity (analogous to $\partial E_i / \partial q_i$), and $J^{Z(i)}$ is an element-specific hardness parameter. This formulation, inspired by charge equilibration methods[55], embeds response-theory structure directly into the energy prediction. The method was demonstrated on the Volmer and Heyrovsky steps of hydrogen evolution on Au(111), with reference data generated using the Solvated Jellium Method in GPAW at the PBE level. Training on approximately 1500 images spanning electrode potentials from 3.8 to 4.6V, the model achieved energy RMSEs of 0.1-0.15 meV/atom and charge RMSEs of 5×10^{-5} electrons/atom on held-out test data. The authors further demonstrated transferability across electrode materials (Pt, Cu, Ag), significant acceleration of nudged elastic band calculations for barrier searches (reducing the number of DFT force calls from 141 to 15 for the initial potential), and the ability to extrapolate from systems with 1-4 explicit water layers to those with 5 layers[53].

Direct learning approaches offer maximum flexibility: they can capture non-linear effects, require no assumptions about response theory, and can potentially interpolate smoothly across the training potential range. However, they are the most data-intensive, requiring DFT calculations across a sufficient range of potentials or charge states to adequately sample the energy surface. Furthermore, extrapolation beyond the training range is not guaranteed to be physically meaningful, unlike response-theory-based methods where the functional form provides some constraints.

4 Challenges

The current challenges in modelling electrified SLI can largely be categorised into a i) data generation bottleneck, ii) standardisation gap and iii) model Architecture and software limitations.

4.1 Data Generation Bottleneck

The data generation challenges were first presented by Govindarajan *et al.* [32] mainly highlighting the fact that different research groups use different codes and modelling approaches (either constant charge or constant potential-based methods). While both approaches have their advantages and drawbacks, this fragmentation prevents aggregation of results across studies to validate and create larger databases. Furthermore, the added computational cost required to describe electrified systems limits the generation of longer trajectories as well as larger systems.

The last decade has seen enormous community effort toward open-access datasets and data standardisation[56,57], driven in large part by the needs of high-throughput screening and machine learning workflows that demand large, coherent, and standardised datasets to benchmark. So far, this revolution has mainly involved bulk materials, giving rise to well-established repositories spanning catalyst discovery and optimisation (OC20[58], The Materials Project[59]), crystal structure prediction (OMC25[60]), organic molecular structure optimisation (OMol25[61]), the AFLOW dataset of material compound and properties[62–64] as well as general-purpose structural databases maintained by specifi groups such as OQMD[65], and Materials Cloud[56]. However, these efforts have been overwhelmingly focused on bulk structures, and no equivalent large-scale collaborative initiative exists for materials interfaces, let alone electrified ones[66]. While some individual groups have begun publishing interface-relevant data[67], these efforts remain sparse and lack standardisation, preventing the cross-study data aggregation that has proven so powerful in bulk materials discovery. Of noteworthy mention are *BeastDB* by Tezak *et al.* [68], which contains single-point DFT calculations of many electrified systems, and LeMat, which aggregates MD trajectories from several projects[69]. However, both remain limited in scope compared to what is needed for systematic interface modelling. We therefore hope that the coming years will see a concerted community effort toward open, standardised datasets for solid-liquid and electrified interfaces, following a similar approach taken for bulk materials simulation data.

4.2 Standardisation Gap

Adhering to the FAIR (Findable, Accessible, Interoperable and Reusable) principles[70] for generation and distribution of data is of utmost importance. In fact, many output files of various MD software (GPAW[71], LAMMPS[72]) are already in a standardised format and are parsable by other tools such ASE[73] as well as various ML packages, where many of the common information (atom type, atom coordination, forces and energies as well as other properties) are readily recognised. However, the added degrees of freedom and information pertaining to global states of the system (e.g. applied potential, work function, number of

View Article Online
DOI: 10.1039/D6LF00149A

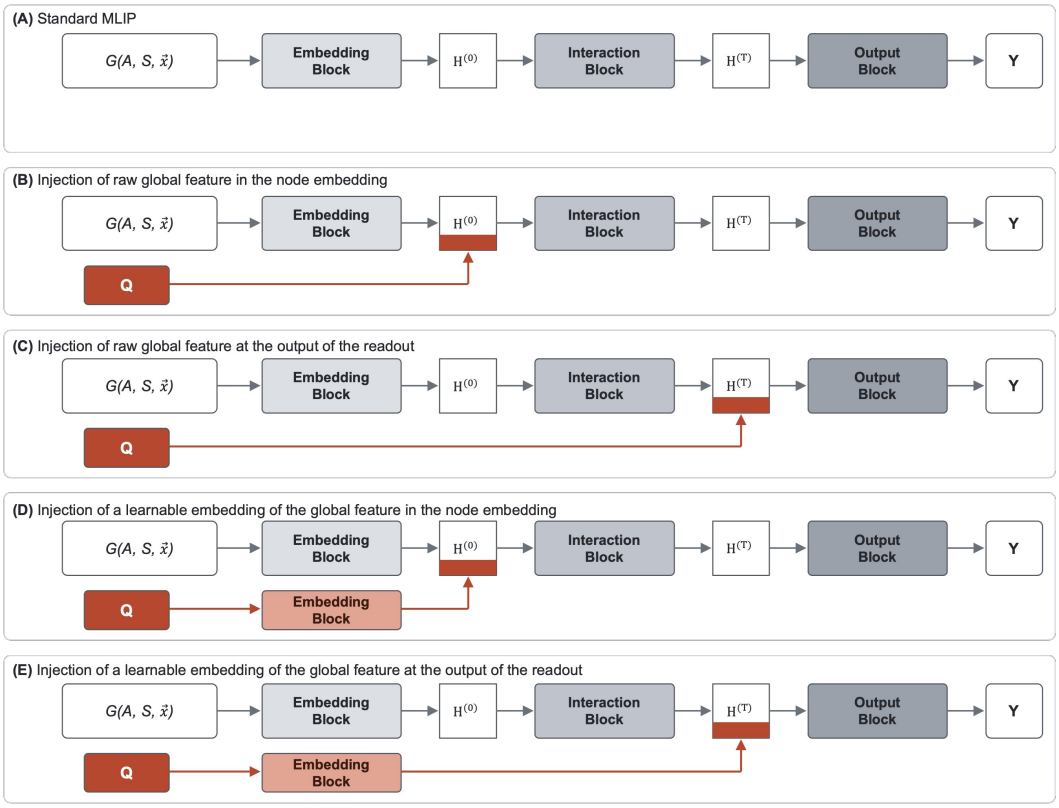

Fig. 1 Different strategies for injection of global system level feature (φ) into a machine learning interatomic potential (MLIP) using a an atomic system representation ($\{Z_i, r_i\}$), where Z_i and r_i is the atomic number and coordinates of atom *i*. A: classical MLIP configuration made of embedding, interaction and output blocks generating a prediction "Y". B: MLIP with injection of φ in the initial node representation ($H(0)$). C: MLIP with injection of φ in the final node representation ($H(T)$). D: MLIP with injection of an embedded representation of φ in the initial node representation ($H(0)$). E: MLIP with injection of an embedded representation of φ in the final node representation ($H(T)$).

electrons, or excess charge) are often not standardised (e.g. consistent variable name, metadata description or scale). There is currently no established convention for how to store and report these quantities: reference scales vary across studies (vs. SHE, vs. RHE, vs. vacuum level), unit conventions for field strength and charge differ, and critical metadata describing the countercharge scheme, solvation model, and boundary conditions employed are often omitted or inconsistently reported. This lack of standardisation could result in confusion and a loss of interoperability across atomic simulation tools as well as ML toolboxes, and ultimately hinders the aggregation of data from different sources into unified training sets. Beyond the lack of formal standardisation there is the issue of interoperability among differnt DFT codes. Different implementation might generate slight different results for the same system. For example the problem was tackled in Ref[74], where a common input/output standard has been designed for internal translation by various workflow managers (AiiDA[75], PerQueue[76], Pipeline Pilot[77], and SimStack[78]), producing a unified schema to enable engine-agnostic workflow execution across CASTEP, GPAW[71], Quantum ESPRESSO[79], and VASP[80].

4.3 Model Architecture and Software Limitations

Absence of standardisation in data reporting expectedly leads incompatible data loading and storage tools, making it difficult to develop generalisable ML pipelines for SLIs[81]. Popular MLIP architectures (MACE[50], NequIP[82] , DeepMD[20], SchNet[83], PAINN[84]) lack native support for global or system-level features. Strategies for incorporating such features are not formalised, tested, and validated. Here, we highlight the work by Wang *et al.*[49], who presented a modification of MACE[50] with two strategies for the inclusion of N_e into the model architecture (see section 3).

Additionally, MD engines that leverage MLIPs, such as ASE[73], LAMMPS[72], and i-PI[85], may not readily propagate the additional system-specific information required for simulating electrified SLIs when interfacing with the underlying potential. Standard MLIPs are designed to output atomic forces for molecular dynamics propagation, where the system evolves deterministically according to Newton's equations of motion. However, achieving a true constant potential (grand canonical) condition requires dynamically adjusting the total electron number of the system, not viable within the continuous trajectory framework of MD. Moreover, varying N_e introduces a fundamental challenge to how standard MLIPs are trained: forces are conservative i.e. the gradient of the predicted total potential energy (Equation 3. Altering N_e means that the total energy E of the system is no longer conserved

View Article Online
DOI: 10.1039/D6LF00149A

along the trajectory.

$$\mathbf{F} = -\nabla_{\mathbf{r}} E(\mathbf{r}, a) \tag{3}$$

Training force-only models could serve as a potential workaround; however, this approach carries its own drawbacks, particularly in the context of MD simulations. Studies have shown that force-only trained MLIPs can lead to failures in conserving energy during NVE dynamics[86], undermining the physical validity of the resulting trajectories.

5 Outlook

Based on the highlighted challenges, we propose a series of potential solutions

5.1 Collaborative Initiatives and Data Generation Strategies

A community effort is needed towards generating simulation data for systems of interest and developing robust frameworks for comparison across methods and modelling strategies[32]. Such initiatives should establish community-agreed schemas for reporting quantities specific to electrified interfaces (analogous to existing conventions for magnetic moments or stress tensors) along with the associated metadata required to ensure data provenance and avoid contamination arising from incompatible methodological choices. Early formation of such standardisation will yield substantial long-term benefits, reducing the need of data harmonisation later as the field matures and datasets grow.

In the absence of community datasets, studies to date have to rely on in-house data generation workflows. These follow similar protocols: i) define the system (slab, solvent, temperature and applied potential), ii) run a short AIMD (typically 10-20 ps), iii) perform time-step filtering i.e. sampling snapshots at fixed interval to ensure the snapshots carry significantly different information and finally iv) extract the properties of interest such as the atom positions, forces and energies.

As more data becomes available and given that there exists a MLIP capable of describing electrified system, it would be possible to employ advanced data generation strategies similar to the case of current MLIPs. Such strategies include the use of computational workflows active learning and ensemble uncertainty to iteratively collect new structures that can contribute to a more diverse dataset[81,87–89]. Ultimately extending the domain of applicability of the MLIPs as well as reducing the associated uncertainty and error[90].

5.2 Flexible MLIP Architectures

One can train separate MLIP for each applied potential (φ) of interest. However, this allows only for limited interpolation and no extrapolation beyond the φ associated with the training. Existing MLIP architectures need to be extended to handle the added degrees of freedom. Expanding the direction proposed by Wang *et al.*[49], we formalise a number of strategies to extend current MLIPs to incorporate global information. To this end, we mainly focus on Graph Neural Networks (GNNs) as the most widely used class of MLIP architectures[91]. The atomic graph as input is described with atomic number Z_i and Cartesian coordinates r_i. The graph representation learning occurs three blocks: an embedding

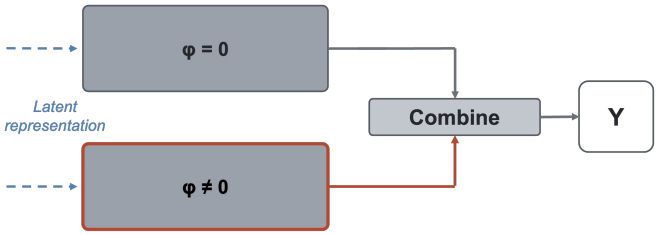

Fig. 2 Alternative approach to account for the presence of applied potential (φ) in atomistic systems. The prediction (Y) is a combination of two output blocks: one accounting for zero potential and the other for the specific applied potential offering a correction to the zero potential head

block (producing an initial representation of the atom, $H^{(0)}$, by embedding the chemical elements of the atoms), an interaction block (where the message-passing (exchange of information between nodes within a cut-off radius), is repeated T times producing the final latent representation $H^{(T)}$) and the output block (responsible for the prediction task, producing the desired outputs Y)[91].

In Figure 1, we present a set of modifications to the standard atomistic learning pipeline (A). We augment an MLIP with global system-level information (here denoted φ) by injecting these quantities to the scalar (invariant) node features either at the output of the embedding block (B) or the output of the interaction block (C).

The global feature can either be used raw, with no prior modification ((B) and (C)), or can be subjected to an embedding operation and produce a higher dimension learnable representation ((D) and (E)).

This conditioning can be applied either at the output of the embedding block (enabling the network to learn global-feature-dependent interatomic interactions during message passing) or at the output of the interaction blocks (allowing global-feature-dependent property prediction).

Wang *et al.*[49] adopted a strategy similar to (B) where MACE[50] was augmented with the number of electrons (N_e). Strategy (D) is similar to (B) with an added embedding/projection layer. Meanwhile Aouichaoui *et al.*[92] adopted a strategy similar to (C) where a global feature in the form of the temperature (T) was concatenated to the readout of a GNN to model temperature dependent properties. Strategy (E) merely expands the dimensionality of the given global feature before concatenation.

An alternative approach could also to be to develop a model at zero applied potential and then leverage the latent representation at zero potential with φ to produce a *correction* to account for the applied potential (see Figure 2).

For the prediction of energy and forces, the model must account for whether the system is conservative or not. As such, other arrangements of the model containing different heads for energy and forces can also be proposed (see Figure 3), with one prediction head for the energy and another for the forces. Here each of the three force components can either be predicted through a multi-task model or single task model (one model for each component).

View Article Online
DOI: 10.1039/D6LF00149A

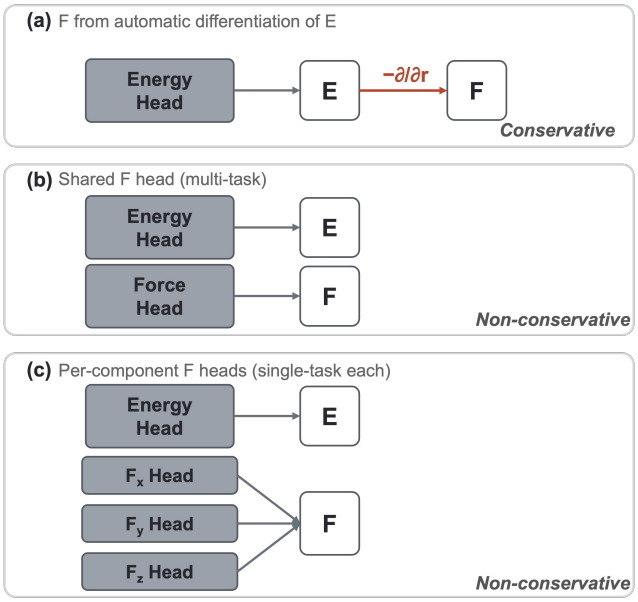

Fig. 3 Different strategies for conducting the prediction of potential energy (E) and forces (F) enacting on the atoms for conservative and non-conservative scenarios

As a next step, it is important to benchmark which strategy for inclusion of global information provides the best accuracy and data/computational efficiency.

5.3 Leveraging Existing Data

Research efforts have predominantly focused on generating simulation data at zero applied potential, resulting in a substantial imbalance between data with and without applied potential. Large-scale initiatives such as Open Catalyst Project (OC25 specifically) [93], and various molecular dynamics trajectory repositories [67,94–101] contain large amount of zero-potential SLI configurations, while electrified interface data remains scarce due to the higher computational expense of constant-potential or finite-field DFT calculations.

It is useful to distinguish three categories of available zero-potential data, ordered by increasing relevance to electrified SLIs:

- (i) Bulk (Materials Project [59], OMat [102], Alexandria [103], MAD [104]) and molecular (OMol [61]) data
- (ii) Surface and adsorbate catalysis data (such as OC20 [58] and OC22 [105])
- (iii) SLI data at zero applied potential (such as OC25 [67,93–101])

The three categories above provide some possibility of large-scale pre-training and transfer learning of models, allowing data-efficient tuning with limited amount of applied potential SLI simulation data.

In practice, transfer learning for electrified SLIs can follow two broad strategies: (a) sequential fine-tuning, where a pre-trained model is adapted to new potential-dependent data, and (b) multi-head architectures, where separate output branches handle different targets. Each strategy manages the risk of catastrophic forgetting (the tendency of fine-tuned models to lose previously learned knowledge [106]) in distinct ways, whether through co-training on mixed datasets or selectively freezing pre-trained layers. We discuss these approaches in detail in the following section.

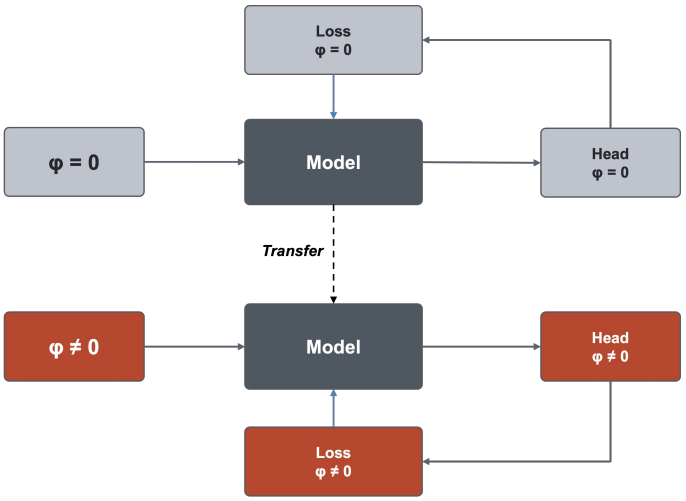

Fig. 4 Transfer learning schema from data with no applied potential (φ) to data with applied potential

5.3.1 Transfer Learning from Zero-Potential Models

GNN training involves learning both graph representations and the prediction model. Zero-potential datasets are helpful in pre-train a GNN such that good representations are learnt although the final prediction targets are not fully compatible with those of electrified SLIs. The pretrained models can be subsequently fine-tuned on electrified data.

This type of transfer learning has already been demonstrated in the literature for non-applied potential work across multiple MLIP architectures, including MACE-MP [107], CHGNet [108], and others, yielding improved accuracy, enhanced training stability of forces and energies, and significant reductions in the required task-specific data. Recent studies have shown that fine-tuning foundation models with partially frozen weights can achieve chemical accuracy using only 10-20% of the data that would be required for training from scratch [109].

For electrified interfaces, a natural two-stage strategy emerges. A model pre-trained on categories (i)-(iii) will have robust elemental and structural embeddings, neighbourhood encodings like short-range interactions that remain largely valid under applied potential. The effect of the electrochemical state can then be viewed as a perturbation to this baseline. Fine-tuning on limited electrified data thus tunes the model's learning capacity in the readout layer on the potential-dependent corrections. A schematic of such an approach can be seen in Figure 4.

Crucially, the choice of *what to freeze* within the model architecture during fine-tuning should reflect where the pre-training data is most informative. Referring to the MLIP architecture presented previously:

- *Embedding block* ($H^{(0)}$): encodes chemical identity into initial node features. When pre training data overs the same

View Article Online
DOI: 10.1039/D6LF00149A

chemical space as the target system, these weights can typically be frozen entirely as element representation are transferable across environments. when using data from (i), the learned embedding block can be partially reused by either acting as an initialization or be temporarily frozen before being rendered trainable.

- *Interaction blocks* ($H^{(0)} \rightarrow H^{(T)}$): encodes interatomic interactions through message passing. If the systems share similar atomic environments, one can opt for freezing the interaction layers completely. If the atomic environments in the systems are too dissimilar then retraining of the message block is needed, possibly after keeping it fixed for a number of initial epochs.

- *Output block*: responsible for predicting the target properties and requires retraining. The reason being that the mapping from latent representations to energies and forces changes when the applied potential introduces new physics not present in the pre-training data.

The domain gap between the pre-training and target data determines the effectiveness of transfer learning. Pre-training on SLI data at zero potential (category (iii)) allows reusing learnt atomic neighbourhood embeddings via messages, and thus message functions can be kept frozen. By contrast, pre-training with surface in vacuum data such as OC20[58]/OC22[105] (category (ii)) includes surface chemistry and adsorbate binding but lacks explicit solvent interactions. So the message passing layers should be retrained as well to learn to represent the solvent structures. Pre-training on bulk data alone (category (i)) provides the least direct transferability to interfacial systems but still offers some useful initialisation for element embeddings and bondings in the solid surface.

5.3.2 Multi-Head Architectures and Joint Training

Compared to sequential transfer learning, multi-head fine-tuning of pre-trained model lowers the risks of catastrophic forgetting with better regularization from the replay task especially when the reference energies are different between the datasets. Rather than full retraining of the readout function, the model trains jointly on both datasets while keeping a shared atomic neighbourhood representation. The embedding and interaction blocks are commonly used to learn the general atomic representations from both dataset, while separate prediction heads specialise for each prediction task one for zero field and one for finite field. This approach is particularly well-suited when one has access to abundant SLI data at zero potential (iii) alongside a smaller set of electrified configurations, since both share the same interfacial chemical environment and differ primarily in the applied field.

Surface catalysis data (ii) is of more limited utility in this context, since vacuum-surface calculations lack explicit solvent and therefore cannot provide training signal for the solvent-metal and ion-metal interactions that dominate the interfacial structure. For the multi-head and joint training, the total loss function can be divided in two contributions:

$$L_{Total} = \lambda_{\varphi=0}\, L_{\varphi=0} + \lambda_{\varphi\neq 0}\, L_{\varphi\neq 0} \tag{4}$$

Where $L_{\varphi=0}$ is a standard MAE (or RMSE) loss function only for the data at zero-potential, while $L_{\varphi\neq 0}$ consider the data at finite field. $\lambda_{\varphi=0}$ and $\lambda_{\varphi\neq 0}$ are tunable parameters.

By maintaining a substantial weight on the zero-potential loss ($\lambda_{\varphi=0} > \lambda_{\varphi\neq 0}$), the model is regularised to preserve the accurate predictions learned from abundant zero-potential data while incrementally incorporating potential-dependent corrections. This is conceptually similar to Elastic Weight Consolidation (EWC)[110] and related continual learning strategies[111], but implemented through explicit multi-task loss weighting rather than parameter-space regularisation.

It is worth noting that the multi-head strategy connects naturally with the delta learning schemes, commonly used in literature to reach computationally expensive high-level of theory reducing the number of required calculations[112–116]: the zero-potential head predicts $\mathbf{E}_{\varphi=0}$ and $\mathbf{F}_{\varphi=0}$, while the finite-field head can be understood as learning the corrections $\delta\mathbf{E}(\varphi)$ and $\delta\mathbf{F}(\varphi)$ on top of the shared latent representation, effectively a learned delta model. This perspective suggests that combining multi-head training with the architectural modifications described in previous sections could further improve data efficiency by explicitly encoding the perturbative structure of the problem. A schematic of this approach can be seen in Figure 5.

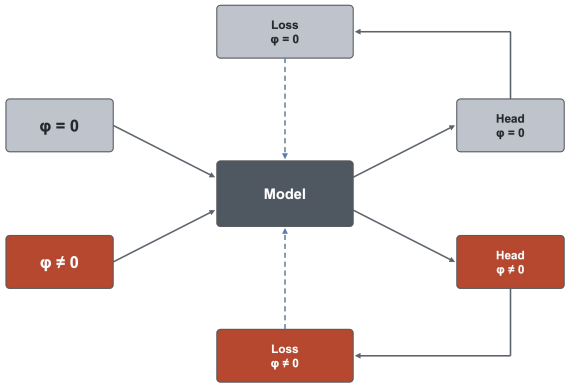

Fig. 5 Multi-head training schema where a model is jointly trained on data with and without applied potential (φ)

Finally, it is worth noting that universal MLIPs[107,117] can serve not only as starting points for transfer learning but also as efficient generators of pre-training data. By running large-scale MD simulations with these universal models on relevant interfacial or bulk systems, one can cheaply produce diverse configurational datasets that augment or replace costly DFT-generated trajectories for the initial training stage. These synthetically sampled configurations can subsequently be selectively refined at the DFT level through active learning, combining the broad configurational coverage afforded by universal MLIPs with the accuracy of first-principles methods where it matters most.

For further details, the reader is referred to a an overview and benchmark of different transfer learning strategies study conducted by Tompa *et al.* [118]

View Article Online
DOI: 10.1039/D6LF00149A

Conclusions

Electrified SLIs are fundamental to many electrochemical processes of relevance to the green transition. With the development of more computationally efficient first-principles methods for simulating systems under applied potential, appropriate modelling of electrified SLIs is becoming viable. In the context of developing MLIPs to study electrified SLIs at longer time scale, we highlight the absence of a unified framework for MLIPs under applied potential as well as other various challenges including data generation bottleneck (due to the computational complexity of the first-principle methods) and the lack of consensus and standardisation of generated data. Going forward, we call for larger collaborative initiatives and to already establish standards and common reference for reporting such data. We also propose a series of flexible templates and easy modifications to current MLIPs to incorporate information about the applied potential that must be investigated in the future to evaluate the best strategy for describing electrified SLIs.

Author contributions

Adem R. N. Aouichaoui: Conceptualization, Formal analysis, Investigation, Methodology, Validation, Visualization, Writing original draft, Writing review and editing
Davide Tisi: Formal analysis, Investigation, Validation, Writing original draft, Writing review and editing
Ivano E. Castelli: Funding acquisition, Resources, Supervision, Writing review and editing
Arghya Bhowmik: Conceptualization, Formal analysis, Project administration, Supervision, Writing review and editing

Conflicts of interest

There are no conflicts to declare.

Data availability

No primary research results, software or code have been included and no new data were generated or analysed as part of this review/perspective.

Acknowledgements

This publication is part of the DECODE project that has received funding from the European Unions Horizon Europe research and innovation programme under grant agreement No 101135537. Views and opinions expressed are however those of the author(s) only and do not necessarily reflect those of the European Union or HADEA. Neither the European Union nor the granting authority can be held responsible for them."

References

1 R. Schlögl, *ChemSusChem*, 2010, **3**, 209–222.
2 M. Khoshkalam, Y. A. Farzin, B. H. Sjølin, C. Spezzati, P. Holtappels, I. E. Castelli and B. R. Sudireddy, *Advanced Engineering Materials*, 2024, **26**, 2302231.
3 J.-B. Le, Q.-Y. Fan, J.-Q. Li and J. Cheng, *Science Advances*, 2020, **6**, eabb1219.
4 S. M. Alfaifi, R. Balu, K. Chiang, N. R. Choudhury and N. K. Dutta, *ACS Catalysis*, 2025, **15**, 9301–9345.
5 A. Kazemi, F. Manteghi and Z. Tehrani, *ACS Omega*, 2024, acsomega.3c07911.
6 J. Shi, Y. Bao, R. Ye, J. Zhong, L. Zhou, Z. Zhao, W. Kang and S. B. Aidarova, *Catalysis Science & Technology*, 2025, **15**, 2104–2131.
7 S. Xu and E. A. Carter, *Chemical Reviews*, 2019, **119**, 6631–6669.
8 X. Zhao, G. Hu, G.-F. Chen, H. Zhang, S. Zhang and H. Wang, *Advanced Materials*, 2021, **33**, 2007650.
9 V. R. Stamenkovic, D. Strmcnik, P. P. Lopes and N. M. Markovic, *Nature materials*, 2017, **16**, 57–69.
10 X. He, D. Bresser, S. Passerini, F. Baakes, U. Krewer, J. Lopez, C. T. Mallia, Y. Shao-Horn, I. Cekic-Laskovic, S. Wiemers-Meyer *et al.*, *Nature Reviews Materials*, 2021, **6**, 1036–1052.
11 S. Shaik, D. Mandal and R. Ramanan, *Nature Chemistry*, 2016, **8**, 1091–1098.
12 C. D. Taylor and M. Neurock, *Current Opinion in Solid State and Materials Science*, 2005, **9**, 49–65.
13 Y. L. Cha, S. Wu, M. S. H. Bijoy, S. M. Taghavi Kouzehkanan, W. Kim, P. Chen, T.-S. Oh, F. Kargar, S. H. Kim and D.-J. Kim, *Journal of Materials Chemistry A*, 2025, **13**, 23816–23825.
14 R. Sechi, G. Kastlunger, A. Bhowmik and H. A. Hansen, *Journal of Chemical Theory and Computation*, 2025, **21**, 5279–5290.
15 D. Bedrov, J.-P. Piquemal, O. Borodin, A. D. J. MacKerell, B. Roux and C. Schröder, *Chemical Reviews*, 2019, **119**, 7940–7995.
16 W. Schmickler, *Chemical Reviews*, 1996, **96**, 3177–3200.
17 S. Ringe and G. Raabe, *Current Opinion in Electrochemistry*, 2025, **51**, 101671.
18 X. Yang, Y. Zhuang, J. Zhu, J. Le and J. Cheng, *WIREs Computational Molecular Science*, 2022, **12**, e1559.
19 V. L. Deringer, A. P. Bartók, N. Bernstein, D. M. Wilkins, M. Ceriotti and G. Csányi, *Chemical Reviews*, 2021, **121**, 10073–10141.
20 H. Wang, L. Zhang, J. Han and W. E, *Computer Physics Communications*, 2018, **228**, 178–184.
21 J. Zeng, D. Zhang, D. Lu, P. Mo, Z. Li, Y. Chen, M. Rynik, L. Huang, Z. Li, S. Shi, Y. Wang, H. Ye, P. Tuo, J. Yang, Y. Ding, Y. Li, D. Tisi, Q. Zeng, H. Bao, Y. Xia, J. Huang, K. Muraoka, Y. Wang, J. Chang, F. Yuan, S. L. Bore, C. Cai, Y. Lin, B. Wang, J. Xu, J.-X. Zhu, C. Luo, Y. Zhang, R. E. A. Goodall, W. Liang, A. K. Singh, S. Yao, J. Zhang, R. Wentzcovitch, J. Han, J. Liu, W. Jia, D. M. York, W. E, R. Car, L. Zhang and H. Wang, *The Journal of Chemical Physics*, 2023, **159**, 054801.
22 A. P. Bartók, M. C. Payne, R. Kondor and G. Csányi, *Physical Review Letters*, 2010, **104**, 136403.
23 J. Behler and M. Parrinello, *Physical Review Letters*, 2007, **98**, 146401.
24 J. S. Smith, O. Isayev and A. E. Roitberg, *Chemical Science*, 2017, **8**, 3192–3203.

View Article Online
DOI: 10.1039/D6LF00149A

25 K. T. Schütt, S. S. P. Hessmann, N. W. A. Gebauer, J. Lederer and M. Gastegger, *The Journal of Chemical Physics*, 2023, **158**, 144801.

26 M. Rupp, A. Tkatchenko, K.-R. Müller and O. A. von Lilienfeld, *Physical Review Letters*, 2012, **108**, 058301.

27 K. T. Butler, D. W. Davies, H. Cartwright, O. Isayev and A. Walsh, *Nature*, 2018, **559**, 547–555.

28 T. W. Ko, J. A. Finkler, S. Goedecker and J. Behler, *Nature Communications*, 2021, **12**, 398.

29 O. T. Unke and M. Meuwly, *Journal of Chemical Theory and Computation*, 2019, **15**, 3678–3693.

30 S. Batzner, A. Musaelian, L. Sun, M. Geiger, J. P. Mailoa, M. Kornbluth, N. Molinari, T. E. Smidt and B. Kozinsky, *Nat. Commun.*, 2022, **13**, 2453.

31 Z. Fan, Z. Zeng, C. Zhang, Y. Wang, K. Song, H. Dong, Y. Chen and T. Ala-Nissila, *Phys. Rev. B*, 2021, **104**, 104309.

32 N. Govindarajan, G. Kastlunger, J. A. Gauthier, J. Cheng, I. Filot, A. Hagopian, H. A. Hansen, J. Huang, P. M. Kowalski, J. Liu, J. M. Lombardi, M. Maraschin, A. Peterson, H. S. Pillai, H. Prats, C. J. Price, R. Van Roij, J. Rossmeisl, R. R. Seemakurthi, S.-J. Shin, A. Smith, J.-X. Zhu and K. Doblhoff-Dier, *ACS Energy Letters*, 2025, 4277–4288.

33 J. Zhou, Y. Fu, L. Liu and C. Liu, *The Journal of Physical Chemistry C*, 2025, **129**, 6414–6422.

34 A. Bhowmik, M. Berecibar, M. Casas-Cabanas, G. Csanyi, R. Dominko, K. Hermansson, M. R. Palacin, H. S. Stein and T. Vegge, *Advanced Energy Materials*, 2022, **12**, 2102698.

35 D. Diddens, W. A. Appiah, Y. Mabrouk, A. Heuer, T. Vegge and A. Bhowmik, *Advanced Materials Interfaces*, 2022, **9**, 2101734.

36 L. G. Verga, S.-J. Shin and A. Walsh, *Current Opinion in Electrochemistry*, 2025, **50**, 101638.

37 J. K. Nørskov, J. Rossmeisl, A. Logadottir, L. Lindqvist, J. R. Kitchin, T. Bligaard and H. Jónsson, *The Journal of Physical Chemistry B*, 2004, **108**, 17886–17892.

38 J. Elsner, K. N. Lausch and J. Behler, *Chemical Physics Reviews*, 2025, **6**, 031310.

39 P. Hou, Y. Tian and X. Meng, *Chemistry A European Journal*, 2024, **30**, e202401373.

40 D. Tang, R. Ketkaew and S. Luber, *Chemistry A European Journal*, 2024, **30**, e202401148.

41 X. Gonze and C. Lee, *Phys. Rev. B*, 1997, **55**, 10355–10368.

42 K. Joll, P. Schienbein, K. M. Rosso and J. Blumberger, *Nature Communications*, 2024, **15**, 8192.

43 S. Falletta, A. Cepellotti, A. Johansson, C. W. Tan, M. L. Descoteaux, A. Musaelian, C. J. Owen and B. Kozinsky, *Nature Communications*, 2025, **16**, 4031.

44 A. Musaelian, S. Batzner, A. Johansson, L. Sun, C. J. Owen, M. Kornbluth and B. Kozinsky, *Nature Communications*, 2023, **14**, 579.

45 Y. Zhang and B. Jiang, *Nature Communications*, 2023, **14**, 6424.

46 C. Feng and B. Jiang, *JACS Au*, 2025, **5**, 5939–5947.

47 C. Feng, Y. Zhang and B. Jiang, *Journal of Chemical Theory and Computation*, 2025, **21**, 691–702.

48 N. Bergmann, N. Bonnet, N. Marzari, K. Reuter and N. G. Hörmann, *Phys. Rev. Lett.*, 2025, **135**, 146201.

49 R. Wang, S. Fang, Q. Huang and Y. Liu, *Journal of Chemical Theory and Computation*, 2025, **21**, 7628–7635.

50 I. Batatia, D. P. Kovacs, G. Simm, C. Ortner and G. Csanyi, Advances in Neural Information Processing Systems, 2022, pp. 11423–11436.

51 M. Sun, B. Jin, X. Yang and S. Xu, *Nature Communications*, 2025, **16**, 3600.

52 L. Zhang, J. Han, H. Wang, R. Car and W. E, *Physical Review Letters*, 2018, **120**, 143001.

53 X. Chen, M. El Khatib, P. Lindgren, A. Willard, A. J. Medford and A. A. Peterson, *npj Computational Materials*, 2023, **9**, 73.

54 J. Behler, *The Journal of Chemical Physics*, 2011, **134**, 074106.

55 A. K. Rappe and W. A. I. Goddard, *The Journal of Physical Chemistry*, 1991, **95**, 3358–3363.

56 L. Talirz, S. Kumbhar, E. Passaro, A. V. Yakutovich, V. Granata, F. Gargiulo, M. Borelli, M. Uhrin, S. P. Huber, S. Zoupanos, C. S. Adorf, C. W. Andersen, O. Schütt, C. A. Pignedoli, D. Passerone, J. VandeVondele, T. C. Schulthess, B. Smit, G. Pizzi and N. Marzari, *Scientific Data*, 2020, **7**, 299.

57 I. E. Castelli, D. J. Arismendi-Arrieta, A. Bhowmik, I. Cekic-Laskovic, S. Clark, R. Dominko, E. Flores, J. Flowers, K. Ulvskov Frederiksen, J. Friis *et al.*, *Batteries & Supercaps*, 2021, **4**, 1803–1812.

58 L. Chanussot, A. Das, S. Goyal, T. Lavril, M. Shuaibi, M. Riviere, K. Tran, J. Heras-Domingo, C. Ho, W. Hu, A. Palizhati, A. Sriram, B. Wood, J. Yoon, D. Parikh, C. L. Zitnick and Z. Ulissi, *ACS Catalysis*, 2021, **11**, 6059–6072.

59 A. Jain, S. P. Ong, G. Hautier, W. Chen, W. D. Richards, S. Dacek, S. Cholia, D. Gunter, D. Skinner, G. Ceder and K. A. Persson, *APL Materials*, 2013, **1**, 011002.

60 V. Gharakhanyan, L. Barroso-Luque, Y. Yang, M. Shuaibi, K. Michel, D. S. Levine, M. Dzamba, X. Fu, M. Gao, X. Liu, H. Ni, K. Noori, B. M. Wood, M. Uyttendaele, A. Boromand, C. L. Zitnick, N. Marom, Z. W. Ulissi and A. Sriram, *Open Molecular Crystals 2025 (OMC25) Dataset and Models*, 2025, `http://arxiv.org/abs/2508.02651`, arXiv:2508.02651 [physics].

61 D. S. Levine, M. Shuaibi, E. W. C. Spotte-Smith, M. G. Taylor, M. R. Hasyim, K. Michel, I. Batatia, G. Csányi, M. Dzamba, P. Eastman, N. C. Frey, X. Fu, V. Gharakhanyan, A. S. Krishnapriyan, J. A. Rackers, S. Raja, A. Rizvi, A. S. Rosen, Z. Ulissi, S. Vargas, C. L. Zitnick, S. M. Blau and B. M. Wood, *The Open Molecules 2025 (OMol25) Dataset, Evaluations, and Models*, 2025, `http://arxiv.org/abs/2505.08762`, arXiv:2505.08762 [physics].

62 C. E. Calderon, J. J. Plata, C. Toher, C. Oses, O. Levy, M. Fornari, A. Natan, M. J. Mehl, G. L. W. Hart, M. Buongiorno Nardelli and S. Curtarolo, *Comp. Mat. Sci.*, 2015, **108**, 233–238.

View Article Online
DOI: 10.1039/D6LF00149A

63 C. Oses, M. Esters, D. Hicks, S. Divilov, H. Eckert, R. Friedrich, M. J. Mehl, A. Smolyanyuk, X. Campilongo, A. van de Walle, J. Schroers, A. G. Kusne, I. Takeuchi, E. Zurek, M. Buongiorno Nardelli, M. Fornari, Y. Lederer, O. Levy, C. Toher and S. Curtarolo, *Comp. Mat. Sci.*, 2023, **217**, 111889.

64 S. Divilov, H. Eckert, S. D. Thiel, S. D. Griesemer, R. Friedrich, N. H. Anderson, M. J. Mehl, D. Hicks, M. Esters, N. Hotz, X. Campilongo, A. Calzolari and S. Curtarolo, *High Entropy Alloys & Materials*, 2025, **3**, 178–187.

65 S. Kirklin, J. E. Saal, B. Meredig, A. Thompson, J. W. Doak, M. Aykol, S. Rühl and C. Wolverton, *npj Computational Materials*, 2015, **1**, 15010.

66 Z. Deng, V. Kumar, F. T. Bölle, F. Caro, A. A. Franco, I. E. Castelli, P. Canepa and Z. W. Seh, *Energy Environ. Sci.*, 2022, **15**, 579–594.

67 Y.-B. Zhuang, C. Liu, J.-X. Zhu, J.-Y. Hu, J.-B. Le, J.-Q. Li, X.-J. Wen, X.-T. Fan, M. Jia, X.-Y. Li, A. Chen, L. Li, Z.-L. Lin, W.-H. Xu and J. Cheng, *Scientific Data*, 2025, **12**, 997.

68 C. Tezak, J. Clary, S. Gerits, J. Quinton, B. Rich, N. Singstock, A. Alherz, T. Aubry, S. Clark, R. Hurst, M. Del Ben, C. Sutton, R. Sundararaman, C. Musgrave and D. Vigil-Fowler, *The Journal of Physical Chemistry C*, 2024, **128**, 20165–20176.

69 A. Ramlaoui, M. Siron, I. Djafar, J. Musielewicz, A. Rossello, V. Schmidt and A. Duval, *LeMat-Traj: A Scalable and Unified Dataset of Materials Trajectories for Atomistic Modeling*, 2025, `http://arxiv.org/abs/2508.20875`, arXiv:2508.20875 [cs].

70 M. D. Wilkinson, M. Dumontier, I. J. Aalbersberg, G. Appleton, M. Axton, A. Baak, N. Blomberg, J.-W. Boiten, L. B. Da Silva Santos, P. E. Bourne, J. Bouwman, A. J. Brookes, T. Clark, M. Crosas, I. Dillo, O. Dumon, S. Edmunds, C. T. Evelo, R. Finkers, A. Gonzalez-Beltran, A. J. Gray, P. Groth, C. Goble, J. S. Grethe, J. Heringa, P. A. T Hoen, R. Hooft, T. Kuhn, R. Kok, J. Kok, S. J. Lusher, M. E. Martone, A. Mons, A. L. Packer, B. Persson, P. Rocca-Serra, M. Roos, R. Van Schaik, S.-A. Sansone, E. Schultes, T. Sengstag, T. Slater, G. Strawn, M. A. Swertz, M. Thompson, J. Van Der Lei, E. Van Mulligen, J. Velterop, A. Waagmeester, P. Wittenburg, K. Wolstencroft, J. Zhao and B. Mons, *Scientific Data*, 2016, **3**, 160018.

71 J. J. Mortensen, A. H. Larsen, M. Kuisma, A. V. Ivanov, A. Taghizadeh, A. Peterson, A. Haldar, A. O. Dohn, C. Schäfer, E. Ö. Jónsson, E. D. Hermes, F. A. Nilsson, G. Kastlunger, G. Levi, H. Jónsson, H. Häkkinen, J. Fojt, J. Kangsabanik, J. Sødequist, J. Lehtomäki, J. Heske, J. Enkovaara, K. T. Winther, M. Dulak, M. M. Melander, M. Ovesen, M. Louhivuori, M. Walter, M. Gjerding, O. Lopez-Acevedo, P. Erhart, R. Warmbier, R. Würdemann, S. Kaappa, S. Latini, T. M. Boland, T. Bligaard, T. Skovhus, T. Susi, T. Maxson, T. Rossi, X. Chen, Y. L. A. Schmerwitz, J. Schiøtz, T. Olsen, K. W. Jacobsen and K. S. Thygesen, *The Journal of Chemical Physics*, 2024, **160**, 092503.

72 A. P. Thompson, H. M. Aktulga, R. Berger, D. S. Bolintineanu, W. M. Brown, P. S. Crozier, P. J. in 't Veld, A. Kohlmeyer, S. G. Moore, T. D. Nguyen, R. Shan, M. J. Stevens, J. Tranchida, C. Trott and S. J. Plimpton, *Comp. Phys. Comm.*, 2022, **271**, 108171.

73 A. Hjorth Larsen, J. Jørgen Mortensen, J. Blomqvist, I. E. Castelli, R. Christensen, M. Duak, J. Friis, M. N. Groves, B. Hammer, C. Hargus, E. D. Hermes, P. C. Jennings, P. Bjerre Jensen, J. Kermode, J. R. Kitchin, E. Leonhard Kolsbjerg, J. Kubal, K. Kaasbjerg, S. Lysgaard, J. Bergmann Maronsson, T. Maxson, T. Olsen, L. Pastewka, A. Peterson, C. Rostgaard, J. Schiøtz, O. Schütt, M. Strange, K. S. Thygesen, T. Vegge, L. Vilhelmsen, M. Walter, Z. Zeng and K. W. Jacobsen, *Journal of Physics: Condensed Matter*, 2017, **29**, 273002.

74 S. K. Steensen, T. S. Thakur, M. Dillenz, J. M. Carlsson, C. R. C. Rêgo, E. Flores, H. Hajiyani, F. Hanke, J. M. G. Lastra, W. Wenzel, N. Marzari, T. Vegge, G. Pizzi and I. E. Castelli, *Advanced Intelligent Discovery*, 2026, **n/a**, e202500232.

75 S. P. Huber, S. Zoupanos, M. Uhrin, L. Talirz, L. Kahle, R. Häuselmann, D. Gresch, T. Müller, A. V. Yakutovich, C. W. Andersen, F. F. Ramirez, C. S. Adorf, F. Gargiulo, S. Kumbhar, E. Passaro, C. Johnston, A. Merkys, A. Cepellotti, N. Mounet, N. Marzari, B. Kozinsky and G. Pizzi, *Scientific Data*, 2020, **7**, 300.

76 B. H. Sjølin, W. S. Hansen, A. A. Morin-Martinez, M. H. Petersen, L. H. Rieger, T. Vegge, J. M. García-Lastra and I. E. Castelli, *Digital Discovery*, 2024, **3**, 1832–1841.

77 J. M. Stevenson and P. D. Mulready, *Journal of the American Chemical Society*, 2003, **125**, 1437–1438.

78 C. R. C. Rêgo, J. Schaarschmidt, T. Schlöder, M. Penaloza-Amion, S. Bag, T. Neumann, T. Strunk and W. Wenzel, *Frontiers in Materials*, 2022, **Volume 9 - 2022**, n/a.

79 P. Giannozzi, S. Baroni, N. Bonini, M. Calandra, R. Car, C. Cavazzoni, D. Ceresoli, G. L. Chiarotti, M. Cococcioni, I. Dabo, A. Dal Corso, S. De Gironcoli, S. Fabris, G. Fratesi, R. Gebauer, U. Gerstmann, C. Gougoussis, A. Kokalj, M. Lazzeri, L. Martin-Samos, N. Marzari, F. Mauri, R. Mazzarello, S. Paolini, A. Pasquarello, L. Paulatto, C. Sbraccia, S. Scandolo, G. Sclauzero, A. P. Seitsonen, A. Smogunov, P. Umari and R. M. Wentzcovitch, *Journal of Physics: Condensed Matter*, 2009, **21**, 395502.

80 G. Kresse and J. Hafner, *Phys. Rev. B*, 1993, **47**, 558(R)–561(R).

81 X. Yang, M. H. Petersen, R. Sechi, W. S. Hansen, S. W. Norwood, Y. Krishnan, S. Vincent, J. Busk, F. R. J. Cornet, O. Winther, J. M. G. Lastra, T. Vegge, H. A. Hansen and A. Bhowmik, *ChemRxiv*, 2024, **2024**,.

82 S. Batzner, A. Musaelian, L. Sun, M. Geiger, J. P. Mailoa, M. Kornbluth, N. Molinari, T. E. Smidt and B. Kozinsky, *Nature Communications*, 2022, **13**, 2453.

83 K. T. Schütt, H. E. Sauceda, P.-J. Kindermans, A. Tkatchenko and K.-R. Müller, *The Journal of Chemical Physics*, 2018, **148**, 241722.

84 K. T. Schütt, O. T. Unke and M. Gastegger, *Equivariant message passing for the prediction of tensorial properties and*

View Article Online
DOI: 10.1039/D6LF00149A

molecular spectra, 2021, https://arxiv.org/abs/2102.03150, Version Number: 4.

85 Y. Litman, V. Kapil, Y. M. Y. Feldman, D. Tisi, T. Begui, K. Fidanyan, G. Fraux, J. Higer, M. Kellner, T. E. Li, E. S. Pós, E. Stocco, G. Trenins, B. Hirshberg, M. Rossi and M. Ceriotti, *The Journal of Chemical Physics*, 2024, **161**, 062504.

86 F. Bigi, M. Langer and M. Ceriotti, *The dark side of the forces: assessing non-conservative force models for atomistic machine learning*, 2024, https://arxiv.org/abs/2412.11569, Version Number: 5.

87 D. Montes De Oca Zapiain, M. A. Wood, N. Lubbers, C. Z. Pereyra, A. P. Thompson and D. Perez, *npj Computational Materials*, 2022, **8**, 189.

88 Y. Zhang, H. Wang, W. Chen, J. Zeng, L. Zhang, H. Wang and W. E, *Computer Physics Communications*, 2020, **253**, 107206.

89 K. Kang, T. A. R. Purcell, C. Carbogno and M. Scheffler, *Phys. Rev. Mater.*, 2025, **9**, 063801.

90 M. Kulichenko, B. Nebgen, N. Lubbers, J. S. Smith, K. Barros, A. E. A. Allen, A. Habib, E. Shinkle, N. Fedik, Y. W. Li, R. A. Messerly and S. Tretiak, *Chemical Reviews*, 2024, **124**, 13681–13714.

91 A. Duval, S. V. Mathis, C. K. Joshi, V. Schmidt, S. Miret, F. D. Malliaros, T. Cohen, P. Liò, Y. Bengio and M. Bronstein, *A Hitchhiker's Guide to Geometric GNNs for 3D Atomic Systems*, 2023, https://arxiv.org/abs/2312.07511, Version Number: 2.

92 A. R. Aouichaoui, A. Cogliati, J. Abildskov and G. Sin, *Computer Aided Chemical Engineering*, Elsevier, 2023, vol. 52, pp. 575–581.

93 S. J. Sahoo, M. Maraschin, D. S. Levine, Z. Ulissi, C. L. Zitnick, J. B. Varley, J. A. Gauthier, N. Govindarajan and M. Shuaibi, *The Open Catalyst 2025 (OC25) Dataset and Models for Solid-Liquid Interfaces*, 2025, https://arxiv.org/abs/2509.17862.

94 X. Yang, A. Bhowmik, T. Vegge and H. A. Hansen, *Chem. Sci.*, 2023, **14**, 3913–3922.

95 A. E. G. Mikkelsen, H. H. Kristoffersen, J. Schiøtz, T. Vegge, H. A. Hansen and K. W. Jacobsen, *Phys. Chem. Chem. Phys.*, 2022, **24**, 9885–9890.

96 X. Tian, A. Tosello Gardini, U. Raucci, H. Xiao, Y. Zhuo and M. Parrinello, *Nature Communications*, 2025, **16**, 10636.

97 L. C. Erhard, J. Schörghuber, A. Comas-Vives and G. K. H. Madsen, *ACS Materials Au*, 2026, **6**, 379–389.

98 J. Schörghuber, N. Buková, E. Heid and G. K. H. Madsen, *Physical Chemistry Chemical Physics*, 2025, **27**, 9169–9177.

99 F. Domínguez-Flores, T. Kiljunen, A. GroSS, S. Sakong and M. M. Melander, *The Journal of Chemical Physics*, 2024, **161**, 044705.

100 A. C. Dávila López, T. Eggert, K. Reuter and N. G. Hörmann, *The Journal of Chemical Physics*, 2021, **155**, 194702.

101 J. Gäding, V. D. Balda, J. Lan, J. Konrad, M. Iannuzzi, R. H. MeiSSner and G. Tocci, *Proceedings of the National Academy of Sciences*, 2024, **121**, e2407877121.

102 L. Barroso-Luque, M. Shuaibi, X. Fu, B. M. Wood, M. Dzamba, M. Gao, A. Rizvi, C. L. Zitnick and Z. W. Ulissi, *Open Materials 2024 (OMat24) Inorganic Materials Dataset and Models*, 2024, https://arxiv.org/abs/2410.12771.

103 T. Cavignac, J. Schmidt, P.-P. De Breuck, A. Loew, T. F. Cerqueira, H. Wang, A. Bochkarev, Y. V. Lysogorskiy, A. H. Romero, R. Drautz, S. Botti and M. A. L. Marques, *Journal of Physics: Materials*, 2026.

104 A. Mazitov, S. Chorna, G. Fraux, M. Bercx, G. Pizzi, S. De and M. Ceriotti, *Scientific Data*, 2025, **12**, 1857.

105 R. Tran, J. Lan, M. Shuaibi, B. M. Wood, S. Goyal, A. Das, J. Heras-Domingo, A. Kolluru, A. Rizvi, N. Shoghi, A. Sriram, F. Therrien, J. Abed, O. Voznyy, E. H. Sargent, Z. Ulissi and C. L. Zitnick, *ACS Catalysis*, 2023, **13**, 3066–3084.

106 J. Kim, J. Lee, S. Oh, Y. Park, S. Hwang, S. Han, S. Kang and Y. Kang, *npj Computational Materials*, 2025, **12**, 26.

107 I. Batatia, P. Benner, Y. Chiang, A. M. Elena, D. P. Kovács, J. Riebesell, X. R. Advincula, M. Asta, M. Avaylon, W. J. Baldwin, F. Berger, N. Bernstein, A. Bhowmik, F. Bigi, S. M. Blau, V. Crare, M. Ceriotti, S. Chong, J. P. Darby, S. De, F. Della Pia, V. L. Deringer, R. Elijoius, Z. El-Machachi, E. Fako, F. Falcioni, A. C. Ferrari, J. L. A. Gardner, M. J. Gawkowski, A. Genreith-Schriever, J. George, R. E. A. Goodall, J. Grandel, C. P. Grey, P. Grigorev, S. Han, W. Handley, H. H. Heenen, K. Hermansson, C. H. Ho, S. Hofmann, C. Holm, J. Jaafar, K. S. Jakob, H. Jung, V. Kapil, A. D. Kaplan, N. Karimitari, J. R. Kermode, P. Kourtis, N. Kroupa, J. Kullgren, M. C. Kuner, D. Kuryla, G. Liepuoniute, C. Lin, J. T. Margraf, I.-B. Magdu, A. Michaelides, J. H. Moore, A. A. Naik, S. P. Niblett, S. W. Norwood, N. ONeill, C. Ortner, K. A. Persson, K. Reuter, A. S. Rosen, L. A. M. Rosset, L. L. Schaaf, C. Schran, B. X. Shi, E. Sivonxay, T. K. Stenczel, C. Sutton, V. Svahn, T. D. Swinburne, J. Tilly, C. van der Oord, S. Vargas, E. Varga-Umbrich, T. Vegge, M. Vondrák, Y. Wang, W. C. Witt, T. Wolf, F. Zills and G. Csányi, *The Journal of Chemical Physics*, 2025, **163**, 184110.

108 B. Deng, P. Zhong, K. Jun, J. Riebesell, K. Han, C. J. Bartel and G. Ceder, *Nature Machine Intelligence*, 2023, **5**, 1031–1041.

109 M. Radova, W. G. Stark, C. S. Allen, R. J. Maurer and A. P. Bartók, *npj Computational Materials*, 2025, **11**, 237.

110 J. Kirkpatrick, R. Pascanu, N. Rabinowitz, J. Veness, G. Desjardins, A. A. Rusu, K. Milan, J. Quan, T. Ramalho, A. Grabska-Barwinska, D. Hassabis, C. Clopath, D. Kumaran and R. Hadsell, *Proceedings of the National Academy of Sciences*, 2017, **114**, 3521–3526.

111 G. M. van de Ven, N. Soures and D. Kudithipudi, in *Continual learning and catastrophic forgetting*, Elsevier, 2025, p. 153168.

112 M. Martyka, J. Jankowska and P. O. Dral, *ChemRxiv*, 2026, **2026**,.

113 L. Gigli, D. Tisi, F. Grasselli and M. Ceriotti, *Chemistry of Materials*, 2024, **36**, 1482–1496.

114 D. Tisi, F. Grasselli, L. Gigli and M. Ceriotti, *Phys. Rev. Mater.*, 2024, **8**, 065403.

View Article Online
DOI: 10.1039/D6LF00149A

115 P. Zaspel, B. Huang, H. Harbrecht and O. A. von Lilienfeld, *Journal of Chemical Theory and Computation*, 2019, **15**, 1546–1559.

116 R. Ramakrishnan, P. O. Dral, M. Rupp and O. A. von Lilienfeld, *Journal of Chemical Theory and Computation*, 2015, **11**, 2087–2096.

117 A. Mazitov, F. Bigi, M. Kellner, P. Pegolo, D. Tisi, G. Fraux, S. Pozdnyakov, P. Loche and M. Ceriotti, *Nature Communications*, 2025, **16**, 10653.

118 T. L. Tompa, E. Varga-Umbrich, I. Batatia, A. M. Elena, N. Bernstein and G. Csányi, *Fine-tuning MLIP foundation models: strategies for accuracy and transferability*, 2026, `https://arxiv.org/abs/2606.12704`.

View Article Online
DOI: 10.1039/D6LF00149A

Data availability

No primary research results, software or code have been included and no new data were generated or analysed as part of this review/ perspective.